IEEE Access
Multidisciplinary | Rapid Review | Open Access Journal

Received September 28, 2021, accepted October 11, 2021, date of publication October 21, 2021, date of current version November 1, 2021.

*Digital Object Identifier 10.1109/ACCESS.2021.3121099*

# Road Surface Wetness Quantification Using a Capacitive Sensor System

**JAKOB DÖRING, ANDREAS BEERING, JULIA SCHOLTYSSEK, AND KARL-LUDWIG KRIEGER**
Institute of Electrodynamics and Microelectronics, University of Bremen, 28359 Bremen, Germany

Corresponding author: Jakob Döring (doering@item.uni-bremen.de)

This work was supported by the German Federal Ministry for Economic Affairs and Energy (BMWi) under Project Sensorsystem zur autonomen Fahrbahnzustandserkennung (SEEROAD) under Grant 19A16016D.

**ABSTRACT** Road surface wetness is a contributing factor in traffic accidents. As the amount of friction reduction correlates with the water film height covering the road surface, a quantification is of high relevance in order to improve traffic safety. Both drivers and autonomous vehicles would benefit from additional information. This paper presents a novel concept for road wetness quantification. It is based on a 2 × 4-planar capacitive transducer array, capable to detect water spray ejected by the tires and its wetness-related dependencies. The reliable assessment of these dependencies by a proposed capacitive sensor system is shown in an experimental study on an asphalt circuit for various wheel speeds. Besides the spray's correlation with speed, the results reveal significant differences in transducer positions and designs confirming the array's relevance regarding wetness quantification. In addition, a 1-nearest neighbor classifier capable of automatically distinguishing between eight wetness levels is proposed. The classifier is optimized by an extended version of balanced accuracy and reaches similar performance as binary classifiers from related research. A balanced ratio between capacitance increase-, standard deviation- and speed-related feature types is one key aspect of classifier performance. Furthermore, up to a certain extent, the array's individual transducers can significantly contribute to classifier performance with design- and position-related advantages.

**INDEX TERMS** Capacitive sensors, driver assistance, road surface wetness detection, vehicle safety, wetness classification.

## I. INTRODUCTION

Although sensor functionality and related driver assistance functions in today's motor vehicles steadily increase, there are still a large number of traffic accidents every year. In 2018, more than 308,000 accidents with personal injury were statistically recorded in Germany, resulting in almost 400,000 casualties [1]. Over two thirds of these accidents were recorded in urban areas and approximately 6% can be ascribed to the road surface condition and weather effects. Here, road surface wetness due to rain is representing more than a third of weather-related accidents.

Due to lower friction between the tires of a vehicle and the road surface, accident risk increases significantly on a wet surface [2]–[4]. The amount of friction reduction depends on the water film height covering the road surface, which can vary between a few microns to a few millimeters [5], [6]. As the water film interferes between tire and road surface, skid resistance is reduced with increasing water film height. Therefore, road surface wetness frequently leads to critical driving situations resulting in accidents.

As former studies on rain-related crashes have shown, the crash frequency increases significantly on wet road surfaces [4]. Since today's vehicles do not provide direct information about the road's current wetness, the vehicle's driver estimates the present conditions intuitively and experience-based. Misinterpretations can lead to fatal consequences for the driver and other traffic participants. Since the amount of skid resistance decreases as vehicle speed increases, speed is a contributing factor in many weather-related accidents [5]. Therefore, speed adjustments are vital to reduce accident risk. Studies on the operating speeds on dry and wet road surfaces could not find a significant speed reduction on wet roads [7]. Drivers do not recognize the lower friction between tires and road surface. Furthermore, in more than 90% of all crashes, driver error is believed to be the main reason, even though

The associate editor coordinating the review of this manuscript and approving it for publication was Salvatore Surdo.

the critical cause is ascribed to the vehicle, environment, or roadway [8].

Autonomous vehicles (AVs), which may be available on the mass market in the near future, are expected to significantly reduce the number of traffic accidents, since driver errors can be eliminated [8], [9]. For environmental perception, different technologies including lidar, radar, and video cameras are commonly used [10]. They allow the vehicle to drive autonomously and additionally to recognize critical situations due to other traffic participants. However, besides a negative impact of adverse weather conditions on environmental sensors, they are unable to detect and quantify road surface wetness [11]–[13]. Therefore, additional sensors for road surface wetness quantification are essential for safe AVs.

In research, several approaches have been studied aiming at the reliable detection of weather-related road conditions. Since modern vehicles are equipped with various cameras as standard, one approach is to use them for that purpose. In [14]–[16] images from both stationary and in-vehicle cameras have been used to classify road surface conditions into different classes including dry, wet, icy, and snowy. Besides being dependent on bright light conditions, they have not yet been able to differentiate between wetness levels. An approach already studied in the 1980s is based on the reflection properties of electromagnetic waves on dry and wet surfaces [17]. Since radar became standard equipment in modern vehicles and costs are approaching an affordable level, research has become more relevant again. The study in [18] for example, shows the possibility to distinguish between dry and wet road surfaces. Similar to in-vehicle cameras, radar does not yet provide a quantification of road surface wetness. Another approach extensively studied in research so far is based on the road surface's optical properties, which change with wetness. The use of a light source and wavelength-selective detectors allows differentiating between wet and dry road surfaces, as shown in [19], [20]. Furthermore, measuring systems based on this approach are commercially available, which provide a quantification of road wetness [21]. However, due to size and cost reasons, they have not yet been suitable for automotive series use.

Research using microphones to record tire-road noise is a further field that has been studied closely. As the noise level differs between a wet and dry road surface, inferences regarding the road condition can be drawn. As shown in [22]–[24] a classification between dry and wet is possible, but so far there has been no differentiation between more than two wetness levels. A more promising approach concerning road wetness quantification is based on structure-borne noise. Water drops impinging on body parts of the vehicle generate noise as structure-borne sound signals, which can be detected by acoustic sensors [25], [26]. As shown in [27] the approach is theoretically suitable to quantify road surface wetness. The Porsche 911 (type 992) has recently been fitted with a sensor of this type. It can detect considerable moisture and is used to warn the driver about the risk of aquaplaning [28], [29]. However, a classification into wetness levels has not yet been reported.

The approach we pursue in this paper is based on the capacitive measuring principle. In the research field of detecting weather-related road conditions, there are only a few publications. Besides stationary capacitive sensors integrated into the roadway [30], a mobile sensor is proposed in [31] which is supposed to detect ice from a remote operated vehicle's underbody. Due to the requirement of a constant low distance to the road surface, it is unsuitable for use in vehicles. In contrast, we use planar capacitive transducers at vehicle body parts as the wheel arch liner to detect impinging water drops thrown up by the tires. As shown in [32], the approach is generally suitable to detect road surface wetness.

In this paper, we focus on a novel concept for the quantification of road surface wetness. Part of this concept is an array comprising various planar capacitive transducers implemented at suitable vehicle body parts. Since transducer selection and positioning are essential to gather adequate information for wetness quantification, we discuss the fundamentals of tire-road interaction and derive a suitable array. In order to prove the reliable assessment of wetness-related dependencies with the introduced concept, we propose a sensor system suited for automotive applications and present an experimental study on a test track. A further focus is on the classification of wetness levels. While the majority of the research presented above only provides differentiation between dry and wet, we present a classifier suitable for the distinction between eight wetness levels. Therefore, we propose a reliable criterion for classifier optimization and evaluate different classifiers for our concept. Additionally, we discuss suitable features and study the transducer array's importance regarding classifier performance.

The remainder of this paper is organized as follows. In Section II, we briefly describe planar capacitive sensors. Afterward, the fundamental concept is described in Section III. Besides the principles of tire-road interaction, the transducer array and the resulting sensor system are presented. Section IV outlines the experimental setup including test vehicle, track, and conditions. Afterward, the experimental results are presented in Section V. In Section VI, we describe the classification. After an introduction of evaluation metrics, we present the classifier optimization. Furthermore, we discuss suitable features and the transducers. Finally, a conclusion is drawn in Section VII.

## II. PRELIMINARIES – PLANAR CAPACITIVE SENSORS

Typically, planar capacitive sensors are made up of two electrodes, the driving electrode and the sensing electrode [33]. Between these electrodes an electric field is applied, penetrating into the medium being monitored. This results in electric displacement inside the medium, altering the charges stored between the electrodes. Thus, sensor capacitance is changed, allowing inferences to be drawn about the medium's permittivity and system parameters that correlate with it.

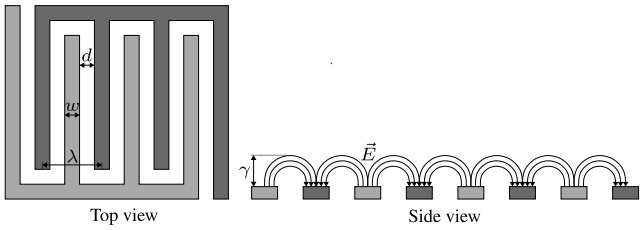


**FIGURE 1.** Schematic representation of an interdigital electrode structure built up by four digits with width $w$, which are separated by a distance $d$.

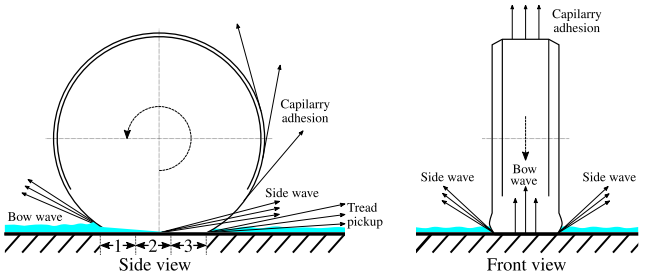


**FIGURE 2.** Three-zone concept of a rolling tire, based on [42] and schematic representation of water ejection on a rotating tire, based on [44]–[46].

In case of the more conventional parallel-plate capacitive sensor, which has the same measuring principle as the planar capacitive sensor, an electric field is distributed uniformly between the two parallel plates [34]. Here, the fringe field is negligible since the electrode surface's dimensions are much larger compared to the electrode thickness. If the arrangement of the electrodes is modified in a manner that creates in-plane electrodes (the parallel electrodes are opened up) the field characteristics will change. The previously negligible fringe field becomes predominant, expanding into the area above the electrodes [33]. Since the electric field lines still penetrate into the medium, single-sided access is provided, which is an essential feature in applications such as the one presented in this paper.

In order to maximize the contribution of the fringing field effect in sensor capacitance, interdigital electrode structures are commonly used to design planar capacitive sensors [35], [36]. The electrodes of these structures are generally built up by the same number of $n$ digits with width $w$, which are separated by a distance $d$ (see Fig. 1). The correlation of width $w$ and distance $d$ can be defined as the distance between the centerlines of adjacent digits belonging to the same electrode. This parameter is denoted as spatial wavelength $\lambda$ in literature and is directly related to the electric penetration depth $\gamma$, which is approximately proportional to it and sometimes defined as one third of it [37], [38]. In addition to $\gamma$, other figures of merit like signal strength, dynamic range, and measurement sensitivity can be adjusted by modifying the introduced parameters. Thus, their choice is essential to meet the application's requirements. Further contributing factors to the figures of merit result from the choice of the manufacturing process and transducer size.

## III. FUNDAMENTAL CONCEPT

In this section, the fundamentals of tire-road interaction are discussed and a suitable transducer array for the quantification of road surface wetness is derived. Furthermore, we propose a capacitive sensor system suited for automotive applications.

### A. TIRE-ROAD INTERACTION

Usually, the contact area between a tire and a wet road surface can be divided into three zones for speeds less than the critical speed of dynamic hydroplaning [39]. The "three-zone concept" was originally suggested by Gough [40] for sliding locked-wheel traction and further carried by Moore [41] to cover the case of a rolling tire [42]. Fig. 2 illustrates the three-zone concept of water displacement by a rolling tire. In the first zone, the tires ride on an unbroken water film while some water is gradually pushed out the sides [43]. The water film becomes progressively thinner in the second zone until it ceases to function as a continuous film [39]. The transition to the third zone is marked by the end of the continuous water film. Here, direct tire to road surface contact is possible through the water film, which facilitates the generation of useful traction.

In order to establish direct contact between tire and road surface, water has to be displaced by the tires as seen for the three-zone concept. There are four primary mechanisms for water ejection by a tire, which are all functions of wheel speed, water film thickness, and tire design [44]–[47]. These mechanisms can be divided into bow and side wave, tread pickup, and capillary adhesion, as illustrated in Fig. 2.

The tire can only transport parts of the total water film on the road surface through the tread grooves to the outside or in direction of the rotation [44], [46]. Thus, the remaining part is displaced ahead of the tire contact area similar to a bow wave, resulting in droplets splashing to the front and the sides. These droplets are large in size and move at comparatively high velocities, which is commonly denoted as "splash" in literature [45], [47]. They follow a ballistic trajectory and generally stay close to the ground. Therefore, bow and side wave usually do not hit the vehicle's surface [48].

Finer droplets with comparatively low velocities, denoted as "spray" in literature, are generated by tread pickup and capillary adhesion [44], [45], [48]. The mechanism of tread pickup occurs due to water being passed through the tread grooves, which is ejected tangentially into the air as soon as centrifugal forces at the rotating wheel exceed adhesion forces [46], [47]. Furthermore, parts of the water under the tire contact area spray away as fine droplets at an angle of less than 30°. The spray can partially contain splash water, which is generally ejected at a shallower angle. Due to capillary adhesion, some water is retained on the tire. It leaves the tire tangentially as fine droplets continuously along the circumference of the tire [49]. For that reason, this kind of spray is sometimes denoted as "circumferential spray" in literature [27]. In the following, we adopt this notation.

**TABLE 1. Specifications of the two manufactured electrode designs.**

| | $A$ [mm$^2$] | $w$ [mm] | $d$ [mm] | $n$ [−] | $\lambda$ [mm] | $\gamma$ [mm] |
|---|---|---|---|---|---|---|
| Design 1 | 50 × 50 | 3.20 | 0.40 | 7 | 7.2 | 2.4 |
| Design 2 | 50 × 50 | 0.63 | 0.63 | 20 | 2.5 | 0.8 |

In contrast to the other effects, which only result from higher road surface wetness, circumferential spray occurs once the road surface is wet [27]. Different factors of influence determine the spray's characteristics. A higher wheel speed results in smaller droplets being ejected at a higher frequency [47]. In contrast, greater road surface wetness leads to bigger droplets up to a certain degree. If the maximum droplet size is reached, greater road surface wetness leads to more droplets. Furthermore, droplet size decreases as the spray-off angle increases due to released water along the rotation. In addition, tire design is another notable factor, since tire depth and geometry determine the amount of water that can stick to the tire after liftoff.

### B. TRANSDUCER ARRAY

In our work, we mainly focus on circumferential spray, as it occurs once the road surface is wet, even at very low wetness levels (see Section III-A). Furthermore, this kind of spray shows a correlation between wheel speed and water film thickness. Thus, vehicle body parts as the wheel arch liners are hit by water droplets of different sizes, amount, and speed. In order to distinguish between various road surface wetness levels, we exploit these dependencies by implementing a transducer array at a suitable position.

For the array layout, we focus on two planar capacitive transducers of the same size, but different electrode design in this work. In Table 1, the specifications of the two electrode designs are summarized. Due to a fixed electrode area $A$, the number of digits $n$ results in two different spatial wavelengths $\lambda$. As described in Section II, varying the spatial wavelength results in differing penetration depths $\gamma$ of the electric field. While Design 1 provides a penetration depth of approximately 2.4 mm, Design 2 only allows the electric field to penetrate around 0.8 mm into the medium due to the lower spatial wavelength. Thus, bigger water droplets and higher amounts lead to faster saturation for Design 2, while Design 1 still allows distinguishing between them. On the other hand, dynamic range and measurement sensitivity behave contrary to penetration depth, as there is a trade-off between these factors. Shortly summarized, Design 1 provides the measurement of water spray in a wider range, while Design 2 is advantageous especially for very low amounts of water droplets.

The two electrode designs are manufactured on flexible printed circuit boards (PCB) as these provide a suitable application on vehicle body parts like the wheel arch liner. The two-layered PCB's base material is made of polyimide (50 µm) and additional adhesive (2 × 15 µm). On top, the electrode structure is realized as copper traces (18 µm) protected by a coverlay made of adhesive (25 µm) and polyimide (25 µm). On the bottom of the base material, a backplane made of copper (18 µm) shields the electrode structure from noise. The bottom is also protected by a coverlay of the same thickness. Summed up, the 54 mm × 54 mm sized transducers have a total thickness of around 0.2 mm. Therefore, they can be applied in a nearly planar manner ensuring a largely unaltered behavior of impinging and draining droplets.

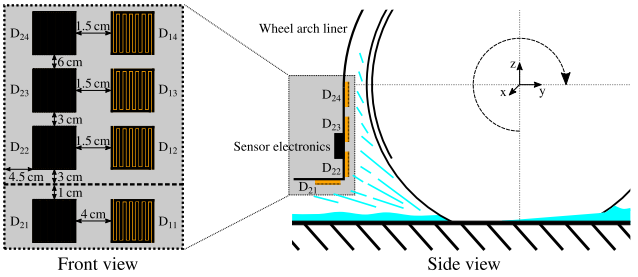


**FIGURE 3. Planar capacitive transducers arranged as a 2 × 4-array on the right front wheel arch liner.**

Since primarily the wheel arch liners are hit by circumferential spray, which also offer an adequate surface area for the transducers, we focus on them for transducer integration. More precisely, we concentrate on the front wheel arch liners' rear-facing sides as these are firstly hit by the spray providing a faster decision regarding road surface wetness. Furthermore, the tires' displacing characteristics lead to modified conditions for the rear wheels causing disadvantages for especially low road surface wetness levels. For implementing the array, we use a total of eight transducers, four of each design (see Table 1), expecting sufficient information for the quantification due to the above-described dependencies. In order to exploit the dependencies and gather enough information, transducer positioning is essential.

The eight transducers are arranged as a 2 × 4-array on the right front wheel arch liner, as shown in Fig. 3. As we neglect the spray's influence in $x$-direction for the selected integration area, we position the two contrary designs adjacent to each other. It is worth mentioning there may be an effect on the spray's characteristics due to steering. This effect is out of the scope of this paper but is not expected to be disadvantageous since steering can be detected and the transducers can complement each other due to their positions. In $z$-direction, the transducers are positioned in one alignment respectively, with exception of $D_{11}$, which is positioned further inside due to constructional reasons. Since droplet size and amount vary along the tire's rotation for circumferential spray and furthermore show a correlation with speed and road surface wetness, we choose four positions one above the other with appropriate distance. While three transducers are positioned at the front wheel arch liner's rear-facing side, one is positioned at the transition to the vehicle's underbody or the side skirt (see Fig. 3). While we expect the lower positioned transducers to

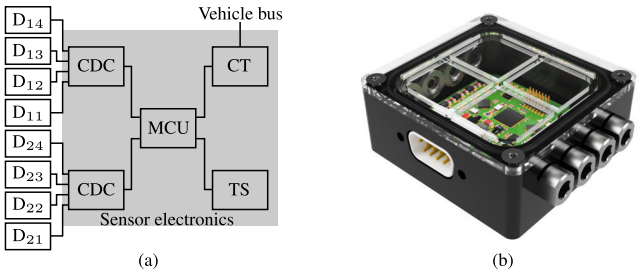


**FIGURE 4.** Block diagram of the capacitive sensor system (a) and sensor electronics mounted in a waterproof housing (b).

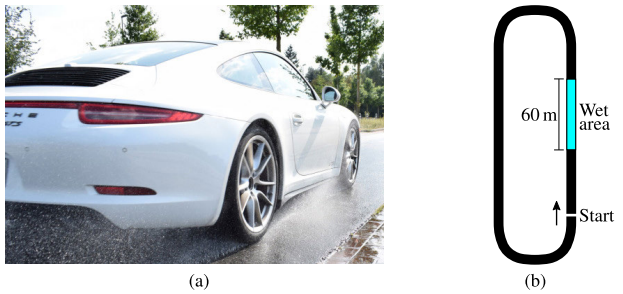


**FIGURE 5.** Test vehicle's tires displacing water resulting in spray (a) on a test track with manual watering option (b).

be more sensitive to lower road surface wetness and wheel speed, we assume these positions to show drawbacks at higher wetness and speed. Circumferential spray might be partially superimposed by other effects (see Section III-A) resulting in high amounts of water. Furthermore, impinging water droplets burst on the wheel arch liner, partially accumulating there and drain off downwards in large drops [46]. These effects can be compensated by the transducers positioned above.

### C. SENSOR SYSTEM

As depicted in Section III-B, we assume a 2 × 4-array of capacitive transducers to be adequate for the quantification of road surface wetness levels. Therefore, sensor electronics have to be designed in a way allowing eight channels to be evaluated almost simultaneously. Fig. 4 (a) shows the sensor system's block diagram. Two capacitance-to-digital converters (CDC) provide the connection of four transducers each. Furthermore, the sensor system includes a temperature sensor (TS) which can be used to compensate for the influence of temperature. The entire control of the program flow is realized by a 32 bit microcontroller (MCU), which has an integrated CAN (Controller Area Network) controller. Thus, the sensor system can be connected to the vehicle bus via a CAN transceiver (CT).

Due to its suitable specifications, the CDC component is realized by FDC2214 from Texas Instruments. FDC2214 provides four channels, a resolution of up to 28 bit, a maximum input capacitance of 250 nF and a maximum output rate of 4.08 ksps [50]. The integrated circuit (IC) uses an LC resonator as a sensor. If the capacitance of a connected transducer changes, the LC resonator's oscillation frequency will be detuned. The IC measures sensor frequency, compares it to a reference frequency, and outputs a digital value proportional to the ratio of sensor and reference frequency. The digital value can be converted to an equivalent capacitance. By tuning the LC resonator, the sensor system's excitation frequency can be defined, which is set to 100 kHz for the experimental study.

The multi-channel sensor electronics, mounted in a waterproof housing, is shown in Fig. 4 (b). Its IP 67 D-SUB connector provides a watertight connection to supply voltage and CAN bus. Furthermore, seals and special cable glands for connecting transducers ensure water tightness. Due to its small size (65 mm × 57 mm × 23 mm), the housing can be positioned behind the wheel arch liner (see Fig. 3) with short connections to the transducers in order to minimize parasitic capacitances.

Since we assume the absolute capacitance to be irrelevant for quantifying road surface wetness, the sensor system transmits the difference between a transducer's current value and the original value of a dry transducer ($\Delta C$) via CAN. The eight capacitances are transmitted within two CAN messages. As one CAN message can transmit 64 bit of data, 16 bit are provided for each capacitance. The implemented configuration results in a value range from -3276.8 pF to 3276.7 pF, a resolution of 0.1 pF and a sampling rate of 145 Hz.

## IV. EXPERIMENTAL SETUP

This section outlines the experimental setup. Besides the test vehicle data, the reference measuring system and its application are presented. Furthermore, test track and studied conditions are introduced.

### A. TEST VEHICLE

The test vehicle is a Porsche 911 (type 991.2 Carrera 4 GTS) with 20 ″ 245/35 winter tires on the front axle, which have a tread depth of approximately 6 mm and an asymmetric tread pattern (see Fig 5 (a)). The vehicle is equipped with a reference measuring system (Lufft, MARWIS) for determining current road surface wetness. It is commonly used as decision support for airports and winter services and can measure water film thickness with non-invasive optical spectroscopy in a range from 0 to 6 mm. It provides a resolution of 0.1 µm, a precision of ±10% and a sampling rate of 100 Hz [21]. For the experimental study, MARWIS is connected via CAN and integrated into the vehicle's front trunk, which is equipped with an opening to the road. Thus, reference data can be recorded synchronous to data from the sensor system and data from the vehicle bus (e.g. wheel speed). Since the opening is located in the vehicle's center, MARWIS' limited sensing area just covers the road surface horizontally shifted to the tire track. Therefore, small deviations regarding the precise water film thickness in the tire track may occur. As we partition water film thickness into wider ranges and furthermore

**TABLE 2. Assignment of road surface wetness levels and water film thickness $t_w$.**

| Road wetness | Class | Water film thickness | $S_{data}$ |
|---|---|---|---|
| Dry | Dry | $0\,\text{mm} \leq t_w < 0.01\,\text{mm}$ | 7812 |
| Damp | $\text{Damp}_1$ | $0.01\,\text{mm} \leq t_w < 0.05\,\text{mm}$ | 2301 |
| | $\text{Damp}_2$ | $0.05\,\text{mm} \leq t_w < 0.10\,\text{mm}$ | 800 |
| Wet | $\text{Wet}_1$ | $0.10\,\text{mm} \leq t_w < 0.20\,\text{mm}$ | 811 |
| | $\text{Wet}_2$ | $0.20\,\text{mm} \leq t_w < 0.30\,\text{mm}$ | 394 |
| | $\text{Wet}_3$ | $0.30\,\text{mm} \leq t_w < 0.40\,\text{mm}$ | 271 |
| Very Wet | $\text{Very Wet}_1$ | $0.40\,\text{mm} \leq t_w < 0.50\,\text{mm}$ | 185 |
| | $\text{Very Wet}_2$ | $0.50\,\text{mm} \leq t_w$ | 98 |

provide a largely homogeneous water film on the test track, these deviations can be neglected.

### B. TEST TRACK AND CONDITIONS

The experimental study is taken on a 445 m long asphalt circuit with two larger straight track sections (see Fig 5 (b)). One of these sections can be watered manually for approximately 60 m. As lower levels of road surface wetness, in particular, cannot be kept stable due to the asphalt's characteristics and the water displacement by the tires, the test track is watered at the beginning of a defined number of test runs, respectively. During these continuous runs, the test track dries to a degree sufficient to cover all defined levels of wetness. Table 2 shows the assignment of road surface wetness levels and water film thickness. Based on thicknesses that realistically occur, we define eight classes ranging from dry to very wet. Especially higher water film thicknesses are hard to realize under given conditions. Even though the scientifically and technically challenging task is to detect low levels of road surface wetness and therefore a larger amount of data is desirable, an imbalanced data set is a result as indicated by $S_{data}$, which describes the number of time windows with a length of 150 sample points (more on this in Section VI). Furthermore, due to the continuous test runs, transducers are not dried. As a result, a certain amount of residual moisture will remain on the transducers potentially complicating road surface wetness quantification.

Besides water film thickness, wheel speed is another dominating factor for circumferential spray (see Section III-A). In this paper, we focus on urban roads and study the corresponding speed range (15 kph, 30 kph and 50 kph). During the test runs (292 in total), wheel speed is kept constant except for the narrow curves. The third notable factor discussed in Section III-A, the tire design, is out of the scope of this paper. Thus, one representative set of tires is tested in the experimental study (see Section IV-A) and the focus is on road surface wetness and wheel speed.

## V. EXPERIMENTAL RESULTS

In order to confirm the assumptions made in Section III-A for the specified speed range and, furthermore, to show the feasibility of quantifying road surface wetness with the introduced concept, we depict representative results in this section. Besides the influence of water film thickness on the measured capacitance, we discuss speed- and position-related differences.

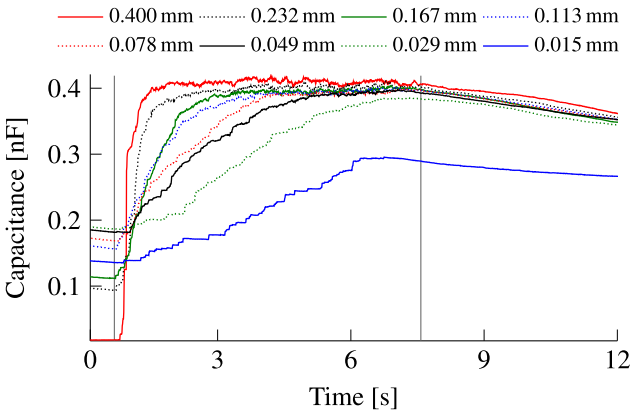


**FIGURE 6. Capacitance against time for varying water film thickness of consecutive test runs at 30 kph (transducer $D_{13}$).**

**TABLE 3. Characteristic parameters of consecutive test runs at 30 kph for transducer $D_{13}$.**

| Water film thickness | $C_{max}$ | $\Delta C_{wet}$ | $\tau_{rise}$ |
|---|---|---|---|
| 0.400 mm | 0.419 nF | 0.391 nF | 0.40 s |
| 0.232 mm | 0.411 nF | 0.308 nF | 0.67 s |
| 0.167 mm | 0.403 nF | 0.288 nF | 1.10 s |
| 0.113 mm | 0.402 nF | 0.243 nF | 1.23 s |
| 0.078 mm | 0.399 nF | 0.228 nF | 1.96 s |
| 0.049 mm | 0.397 nF | 0.214 nF | 2.27 s |
| 0.029 mm | 0.385 nF | 0.197 nF | 3.47 s |
| 0.015 mm | 0.295 nF | 0.159 nF | 3.98 s |

Fig. 6 exemplarily shows characteristic capacitance curves for varying water film thickness (WFT) of consecutive test runs at 30 kph. Since Design 1 provides the measurement of water spray in a wider range (see Section III-B), the curves are shown for transducer $D_{13}$ (see Fig. 3). The water film thickness indicated in the legend represents the mean value over the entire wet section of approximately 60 m (marked by vertical lines), measured with reference measuring system MARWIS. In addition, Table 3 summarizes characteristic parameters of the capacitance curves for these test runs.

In general, the capacitance increases immediately after entering the wet area due to impinging water droplets generated by the tires. As circumferential spray, which is the dominant spray type for the wheel arch liners (see Section III-A), is correlated with water film thickness, significant differences between wetness levels occur. With decreasing road surface wetness, droplet amount and size decrease, resulting in differing capacitance curves and characteristics. The maximum capacitance $C_{max}$ only differs slightly for medium wetness levels, but shows a decreasing trend over the entire wetness range of the consecutive test runs on that transducer position. Furthermore, the capacitance curves' gradient significantly

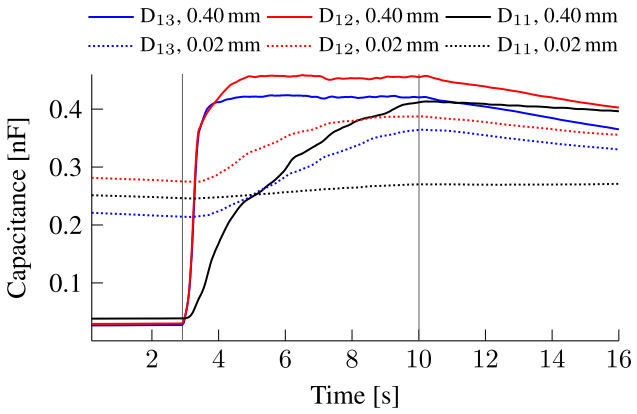


**FIGURE 7.** Mean capacitance against time for two wetness levels and three transducer positions at 30 kph.

**TABLE 4.** Characteristic parameters of two wetness levels and three transducer positions at 30 kph.

| WFT | Transducer | $C_{\max}$ | $\Delta C_{\text{wet}}$ | $\sigma_{\max}$ | $\tau_{\text{rise}}$ |
|---|---|---|---|---|---|
| 0.40 mm | $D_{13}$ | 0.424 nF | 0.392 nF | 0.024 nF | 0.40 s |
| | $D_{12}$ | 0.458 nF | 0.425 nF | 0.032 nF | 0.41 s |
| | $D_{11}$ | 0.413 nF | 0.373 nF | 0.060 nF | 2.70 s |
| 0.02 mm | $D_{13}$ | 0.365 nF | 0.149 nF | 0.023 nF | 4.06 s |
| | $D_{12}$ | 0.387 nF | 0.112 nF | 0.036 nF | 2.93 s |
| | $D_{11}$ | 0.271 nF | 0.024 nF | 0.059 nF | 4.18 s |

declines with decreasing water film thickness. While time constant $\tau_{\text{rise}}$, which indicates the time needed from the wet section's start to reach 63.2% of the measured capacitance at the wet section's end, is small for the first measurement it almost increases tenfold to the last one allowing to distinguish between wetness levels. When exiting the wet area, capacitance decreases as no more droplets impinge and water drains off downwards the wheel arch liner. Due to the continuous test runs, residual moisture remains on the transducers showing up as a capacitance offset at the beginning of a measurement (similar to condensation or contamination). However, despite that drawback, a distinction between wetness levels is still possible since the capacitance increase is significant, as indicated by $\Delta C_{\text{wet}}$, which describes the capacitance difference between entrance and exit of the wet section.

In Fig. 7, mean capacitance curves for two wetness levels and three different transducer positions at 30 kph are shown. In order to show the position's influence on the measured capacitance, transducers $D_{11}$ to $D_{13}$ are exemplarily selected for the comparison. While $D_{11}$ is positioned at the transition to the vehicle's underbody, the other two are positioned above each other at the front wheel arch liner's rear-facing side (see Fig. 3). In each case, the mean capacitance is determined from seven test runs with similar water film thickness (±0.015 mm). Additionally, Table 4 summarizes related parameters, including maximum standard deviation $\sigma_{\max}$ inside the wet section.

Each transducer position shows considerable capacitance difference between the two selected water film thicknesses for both $C_{\max}$ and $\Delta C_{\text{wet}}$. Therefore, the above conclusions also apply to these positions. In comparison to each other, position-related differences can be observed. As droplet size and amount vary along the tire's rotation for circumferential spray, the spray's influence on transducer $D_{12}$ is bigger than on transducer $D_{13}$, which is positioned above in $z$-direction. As a result, maximum capacitance is significantly higher for transducer $D_{12}$ in both cases. On the other hand, the upper position has advantages regarding residual moisture, as water drains off downwards the wheel arch liner. Thus, the transducer dries faster resulting in a lower capacitance offset at the beginning of measurement as can be seen for a water film thickness of 0.02 mm. Furthermore, this results in a larger $\Delta C_{\text{wet}}$ for transducer $D_{13}$ even though impinging droplet size and amount are lower. Considering time constant $\tau_{\text{rise}}$, only minimal difference is noticeable for high road surface wetness since the amount and size of impinging droplets are high for both transducers resulting in a fast reaching of the position-related maximum. On the contrary, in the case of low road surface wetness $\tau_{\text{rise}}$ is smaller for $D_{12}$ as available water along the tire's rotation becomes noticeably less and in addition, residual moisture is higher.

Due to its position at the transition to the vehicle's underbody, $D_{11}$'s behavior differs. At a water film thickness of 0.4 mm both $C_{\max}$ and $\Delta C_{\text{wet}}$ are smaller in comparison to $D_{12}$ and $D_{13}$. An even more significant difference arises for $D_{11}$'s $\tau_{\text{rise}}$, which is more than six times larger compared to the others. Although a high amount of water is whirled up by the tires, a comparably small percentage of it impinges on the transducer. Furthermore, when exiting the wet area, the capacitance continues to increase slightly due to draining and dripping water. For a water film thickness of 0.02 mm a similar behavior can be observed. Even though the time constants are less far separated, the capacitance increase is comparably small. Due to its horizontal position, the transducer is less attracted to impinging water droplets in the studied speed range. Nevertheless, $D_{11}$ can complement significantly to the transducer array since its redundancy to the other transducers is low, even though the stochastic component of the impinging water droplets is larger, as $\sigma_{\max}$ indicates.

Fig. 8 shows mean capacitance curves for three wetness levels of different classes and three wheel speeds for transducer $D_{13}$. In order to compare the studied vehicle speeds, the capacitance curves are plotted against distance displaying a section of 40 m. In addition, Table 5 summarizes characteristic parameters of these results.

All capacitance curves of the studied wheel speeds show a similar behavior regarding declining road surface wetness. While both $C_{\max}$ and $\Delta C_{\text{wet}}$ decrease within a wheel speed, $\tau_{\text{rise}}$ increases due to reducing droplet amount and size allowing to differentiate between wetness levels. Therefore, the above conclusions regarding the correlation with water film thickness equally apply to different wheel speeds. As circumferential spray is also correlated with wheel

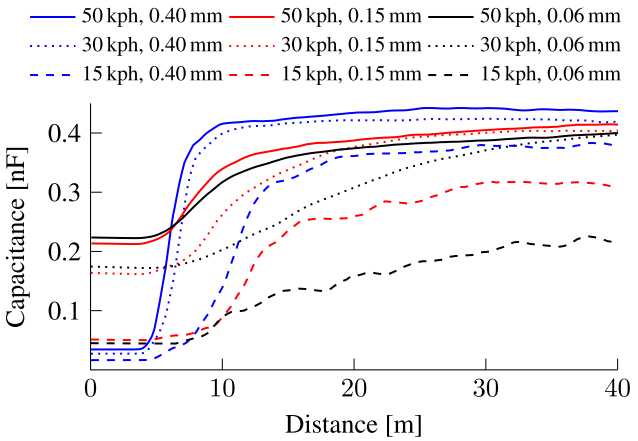


**FIGURE 8.** Mean capacitance against distance for three wetness levels and three wheel speeds for transducer $D_{13}$.

**TABLE 5.** Characteristic parameters for three wetness levels and three wheel speeds for transducer $D_{13}$.

| WFT | $v_{\text{wheel}}$ | $C_{\max}$ | $\Delta C_{\text{wet}}$ | $\sigma_{\max}$ | $\tau_{\text{rise}}$ |
|---|---|---|---|---|---|
| 0.40 mm | 50 kph | 0.443 nF | 0.407 nF | 0.021 nF | 0.23 s |
| | 30 kph | 0.424 nF | 0.393 nF | 0.024 nF | 0.40 s |
| | 15 kph | 0.383 nF | 0.367 nF | 0.047 nF | 2.37 s |
| 0.15 mm | 50 kph | 0.423 nF | 0.207 nF | 0.011 nF | 0.45 s |
| | 30 kph | 0.409 nF | 0.244 nF | 0.043 nF | 1.05 s |
| | 15 kph | 0.318 nF | 0.267 nF | 0.082 nF | 2.93 s |
| 0.06 mm | 50 kph | 0.419 nF | 0.196 nF | 0.010 nF | 0.65 s |
| | 30 kph | 0.405 nF | 0.229 nF | 0.031 nF | 1.97 s |
| | 15 kph | 0.226 nF | 0.180 nF | 0.059 nF | 5.14 s |

speed, a comparison of the studied speeds shows significant differences between the capacitance curves and their characteristic parameters. Due to droplets being ejected at a higher frequency, resulting in larger amounts, $C_{\max}$ is generally larger for greater wheel speeds within one water film thickness while $\tau_{\text{rise}}$ is smaller. On the contrary, $\Delta C_{\text{wet}}$ shows different behavior for lower wetness levels. Due to faster test laps at higher wheel speeds, the amount of residual moisture remaining on the transducers is frequently larger. Thus, a higher capacitance offset is noticeable at the start of a measurement, which reduces the capacitance range to the speed-related maximum and results in smaller values for $\Delta C_{\text{wet}}$, even though the amount of impinging droplets is higher. Furthermore, $\sigma_{\max}$ rises with decreasing wheel speed as the potential capacitance range gets wider due to a lower amount of droplets available.

In brief, the assumptions made in Section III-A regarding tire spray can be confirmed for the studied wheel speeds. Circumferential spray shows a correlation with both road wetness and wheel speed. Thereby, the amount and size of thrown up water droplets differ. As droplet size and amount furthermore vary along the tire's rotation, transducer position-related differences occur. As has been shown, the capacitive sensor system is suitable to meet the requirements for detecting circumferential spray and its correlation induced changes. Thus, various wetness levels at different wheel speeds can be detected, even in extreme scenarios as very little road surface wetness at low wheel speed.

## VI. CLASSIFICATION

In this section, the focus is on road surface wetness classification. In Section VI-A, suitable metrics for classifier optimization and assessment are introduced. Section VI-B covers the evaluation of classifier algorithms and optimization criteria. In Section VI-C, the selected features and in Section VI-D the array's transducers are discussed.

### A. EVALUATION METRICS

In order to automatically classify road surface wetness, measurement data is split up into time windows with a length of 150 sample points and labeled into eight classes ranging from dry to very wet (see Section IV-B). As a result, each class comprises a specific number $S_{\text{data}}$ of time windows, summarized in Table 2. According to the table, the resulting data set is imbalanced, since especially higher wetness levels are hard to realize under given conditions. As most classifier learning algorithms assume a balanced distribution and equal miscalculation costs, small classes are misclassified more often [51]–[53]. At the data-level, solutions for imbalanced data sets, such as randomly oversampling the small class or undersampling the prevalent class, are possible. Due to the data set size and in order to prevent overfitting, we refrain from adjusting the data set. Instead, we choose suitable evaluation metrics for measuring performance and optimizing the classifier.

The choice of evaluation metrics is crucial in order to assess the classifier's performance correctly. Furthermore, an accurate metric is essential to optimize the classifier. The most commonly used evaluation metric is the accuracy, which is defined as the ratio of correctly classified samples and the overall number of samples [51], [54]. For an imbalanced data set, accuracy tends to be biased towards the majority class as smaller classes have only little impact on it [52], [53]. Thus, other adequate metrics taking the class distribution into account are more suitable for these problems.

A commonly used metric in practice is the balanced accuracy (BAC), which has conceptual strengths compared to conventional accuracy while maintaining its simplicity [55]. BAC can take values in the range of [0, 1], where 1 represents the perfect classification. It is defined as the recall obtained of each class averaged over the number of classes [56], [57]

$$\text{BAC} = \frac{1}{N} \cdot \sum_{i=1}^{N} \text{recall}_i, \tag{1}$$

where $N$ is the number of classes. The recall, which describes the proportion of positive labeled cases correctly classified, is defined as

$$\text{recall}_i = \frac{\text{TP}}{\text{TP} + \text{FN}}, \tag{2}$$

where TP represents the number of correctly predicted positive labeled cases (true positive) and FN the number of positive cases misclassified as negative cases (false negative). Some variations of the recall have already been used by many systems to optimize and evaluate classifiers [54]. Since we assume misclassifications to adjacent classes as less safety relevant (except between dry and $\text{damp}_1$), we extend the classes' $\text{recall}_i$ by an additional weighting factor

$$\text{recall}_i^* = \text{recall}_i \cdot \frac{\text{TP} + \frac{1}{2} \cdot \Phi\,(\text{FN})}{\text{TP}}, \tag{3}$$

where $\Phi\,(\text{FN})$ represents the number of false negatives in adjacent classes. For the above reasons, misclassifications between dry and $\text{damp}_1$ are not taken into account and are therefore not considered in $\Phi\,(\text{FN})$. Accordingly, also the balanced accuracy (see eq. 1) is extended, which is referred to as BAC* below.

In addition, we consider a further reliable evaluation metric, the Matthews correlation coefficient (MCC), for comparison reasons in this paper. MCC was originally developed for binary tasks in [58] and extended to multiclass problems in [59]. It represents a metric that has been proven to be appropriate for performance evaluation and classifier optimization in case of imbalanced data sets [53], [60]. MCC can take values in the range of $[-1, 1]$, where 1 represents the perfect classification. It is defined in eq. 4, where $C$ is an $N \times N$ confusion matrix, whose $kl$-th entry $C_{kl}$ represents the number of elements of true class $k$ that have been assigned to class $l$ by the classifier [56], [60]. In this paper, we consider the introduced metrics for both classifier assessment and optimization.

### B. CLASSIFIER OPTIMIZATION

In order to find a suitable classifier for quantifying road surface wetness into eight classes, a reliable learning algorithm is required. In research, there is no documented standard way for classifying road surface conditions [15]. Furthermore, existing classifiers in this application field have largely only provided a differentiation between dry and wet. Since we additionally use a new approach for road surface wetness detection, we study two conventional learning algorithms to our data set which have already been successfully applied to many application domains including road surface condition classification [24], [51], [61]. One algorithm is the decision tree (DT) which is one of the most intuitive and frequently used ones in data science [62]. To divide a data set into predefined classes it uses a flowchart-like tree structure [63]. The other algorithm applied in this paper is the $k$-nearest neighbors (KNN) classifier which often comes surprisingly close to the optimal Bayes classifier and works well on many problems [64]. To predict a class, KNN identifies $k$ points in training data with the smallest distance to the test sample to be assigned. In order to define the distance KNN uses an appropriate metric. In this paper, we apply Euclidean distance which is a commonly used metric that has shown comparatively good results [65]. Furthermore, the choice of $k$ is essential for an optimal KNN classifier. Although expensive in terms of computation time, one reliable way to determine $k$, which we also follow, is to perform cross-validation tests with various values and select the best one, which often yields excellent predictive performance [66].

Due to the limited data set, we use tenfold cross-validation for evaluating the classifiers, which involves randomly dividing the data into ten folds of approximately equal size [64]. Each fold serves once as validation data and the remainder for training. Although other numbers of folds are possible, tenfold cross-validation has become the standard method in practical turns since extensive tests on numerous data sets and algorithms have shown that it provides the best error estimation [57], [66]. In addition, we use sequential forward selection (SFS) to choose relevant features from our set with 593 features. Thus, besides the improvement of training speed and prediction performance, avoidance of overfitting can be ensured [62], [67]. SFS is a bottom-up search procedure incrementally adding features selected by an evaluation metric to an empty feature set [68]. For that purpose, we use the three metrics presented in Section VI-A. In the following, we refer to the metric used to identify relevant features as optimization criterion (OC) and to the one that is used to assess the performance as evaluation criterion (EC).

**TABLE 6. Mean and best classifier performance of tenfold SFS with regard to the optimization criterion.**

| OC \ EC | | BAC | | BAC* | | MCC | |
|---|---|---|---|---|---|---|---|
| | | DT | 1NN | DT | 1NN | DT | 1NN |
| BAC | mean | 0.7989 | 0.8359 | 0.8550 | 0.8574 | 0.7894 | 0.8105 |
| | best | 0.8153 | 0.8403 | 0.8680 | 0.8702 | 0.8052 | 0.8185 |
| BAC* | mean | 0.7941 | 0.8540 | 0.8551 | 0.8779 | 0.7830 | 0.8366 |
| | best | 0.8221 | 0.8944 | 0.8728 | 0.9204 | 0.8133 | 0.8880 |
| MCC | mean | 0.8010 | 0.8439 | 0.8576 | 0.8684 | 0.7929 | 0.8273 |
| | best | 0.8234 | 0.8670 | 0.8770 | 0.8963 | 0.8178 | 0.8613 |

$$\text{MCC} = \frac{\sum_{k,l,m=1}^{N} C_{kk}C_{lm} - C_{kl}C_{mk}}{\sqrt{\sum_{k=1}^{N}\left[\left(\sum_{l=1}^{N} C_{kl}\right)\left(\sum_{\substack{l',k'=1 \\ k'\neq k}}^{N} C_{k'l'}\right)\right]}\sqrt{\sum_{k=1}^{N}\left[\left(\sum_{l=1}^{N} C_{lk}\right)\left(\sum_{\substack{l'k'=1 \\ k'\neq k}}^{N} C_{l'k'}\right)\right]}} \tag{4}$$

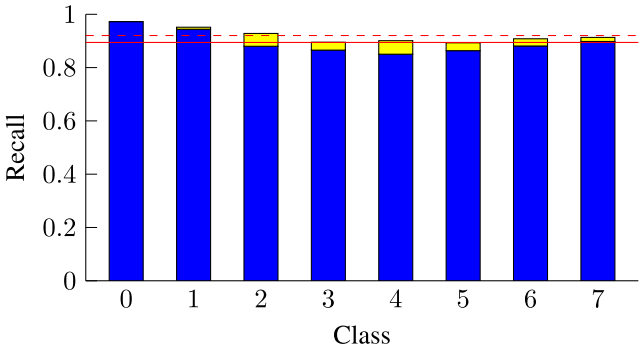


**FIGURE 9.** The eight classes' recall (blue) and extended recall (blue and yellow) of 1NN classifier with BAC* as OC, resulting in a BAC of 0.89 (solid line) and a BAC* of 0.92 (dotted line).

With regard to the classifier assessment, each learning algorithm (DT, KNN where $1 \leq k \leq 15$) is studied tenfold with each OC to increase the results' confidence. Thus, both algorithms and OCs can be evaluated. In Table 6 mean and best values of the ten iterations are summarized. The term best refers to the SFS with the highest classifier performance. Since 1NN has shown top performance for all OCs, we refrain from displaying other values of $k$ for overview purposes. As shown in the table, 1NN outperforms DT for both mean and best regardless of the OC, indicating its superior suitability for the present application. Furthermore, significant variations between the resulting SFSs can be deduced from the table. Since SFS can be considered a greedy approach, it does not necessarily yield the globally optimum solution resulting in significant variations [62]. Therefore, the probability of identifying an optimal SFS can be increased by performing several iterations.

According to the results presented in Table 6, BAC* shows advantages as OC in comparison to BAC and MCC for classifier optimization. Selecting BAC* as OC even results in higher BAC and MCC performances than with OC equal to EC. While the best 1NN optimized with BAC yields a BAC of 0.84, the optimization with BAC* results in a BAC value of 0.89. Similar behavior can be noticed for the MCC. Here, the difference between the two MCC performances is almost 0.03 with an advantage to BAC* as OC. Thus, the extended balanced accuracy is the most suitable optimization criterion for the studied classifier algorithms under given conditions resulting in a 1NN classifier with BAC* performance of 0.92.

Fig. 9 shows the 1NN classifier's recall (blue bars) for the eight classes, where 0 represents dry and 7 very wet$_2$. In combination with the part stacked upon it, this results in the extended recall. In addition, the solid line shows the recall's mean (BAC) and the dashed one the extended recall's mean (BAC*). According to the figure, all classes exceed a recall of 0.83, respectively a recall* of 0.86, resulting in largely balanced class distribution. Furthermore, it is noticeable that especially classes 2-6 benefit from the extension of recall, as these classes tend to misclassify into neighboring classes more frequently. As outlined in Section V, this can be attributed to the capacitance curves' characteristics which are partially similar for medium wetness levels. In addition, another factor is to be found in the narrow classes and small time windows.

The figure also reveals that recalls of classes dry (0.97) and damp$_1$ (0.94) are significantly higher. A potential source of influence might be the classes' greater number of time windows $S_{\text{data}}$ (see Table 2). As the training set is larger, pattern recognition is more reliable than in smaller classes where generalizations are more difficult. On the other hand, these classes also show a different behavior regarding the capacitance curves' characteristics, since none or only little amounts of water droplets hit the transducers. Thus, a more clear distinction from the other classes is possible resulting in higher classification performance. Since damp$_1$ in particular is hard to detect from a measurement point of view, these results demonstrate the potential of our approach and the resulting classifier. Prospectively, new training data can improve the results and are also desirable for a new system configuration or driving scenarios.

Due to the novel concept, the rare publications on road wetness classification, and the fact that the majority only differentiates between dry and wet, it is only possible to compare the above results with those from related research to a limited extent. Nevertheless, we put them into context with the findings of two other publications that have also classified road surface wetness for the relevant speed range. In [22] road surface wetness is detected from the audio of tire-surface interaction in an experimental study and different classifiers are presented. The best classifier yields a BAC of 0.93 and can differentiate between dry and wet. Similar results are presented in [24]. The acoustic measurements can be classified into dry and wet with a BAC of 0.93 as well. Furthermore, another classifier capable to distinguish between dry, damp, and wet with a BAC of 0.82 is presented in [24]. In comparison, the above-presented classifier yields a BAC of 0.89. Thus, the classifier's BAC is slightly below the two compared binary classifiers' performance, but above the three-class one's and provides decent results. As shown above, the classes dry and damp$_1$ yield a high performance. Therefore, a binary version of the presented classifier can be assumed to perform particularly well for our approach. In order to prove that, we merge seven classes and develop a binary 1NN classifier based on the findings above. The resulting classifier yields a BAC of 0.998 confirming the ability of our approach to almost perfectly distinguish between a dry and wet road surface.

### C. FEATURE EVALUATION

One key aspect of the classifier performance can be attributed to the features selected by SFS. In order to evaluate the features' importance with regard to classifier performance, we take a closer look at them in this section. For that purpose, we concentrate on the most promising classifier algorithm evaluated in Section VI-B, the 1NN with BAC* as OC.

**TABLE 7. Overview of the feature set for each transducer.**

| Statistics | $C$ | $\frac{\partial C}{\partial t}$ | $\frac{C}{v}$ | $\frac{\partial \frac{C}{v}}{\partial t}$ | $v$ |
|---|---|---|---|---|---|
| max, min | • | • | | • | |
| mean | • | • | • | | • |
| median, SD, variance, signal energy, RMS, skewness, kurtosis, delta, $\frac{\mathrm{SD}_s}{\mathrm{mean}_s}\Big\vert_{\max}$, $\frac{\mathrm{SD}_s}{\mathrm{mean}_s}\Big\vert_{\min}$, $\frac{\mathrm{SD}_s}{\mathrm{mean}_s}\Big\vert_{\mathrm{mean}}$, $\mathrm{diff}_{\max}$, $\mathrm{diff}_{\min}$ | • | | | | |
| range | • | | | • | |
| $\mathrm{magnitude}_{\max}$ | | • | | | |
| $\mathrm{largest/smallest\ values}_{s\%,\mathrm{mean}}$, $\mathrm{SD}_{s,\max}$, $\mathrm{SD}_{s,\min}$, $\mathrm{SD}_{s,\mathrm{mean}}$ | • | | • | | |

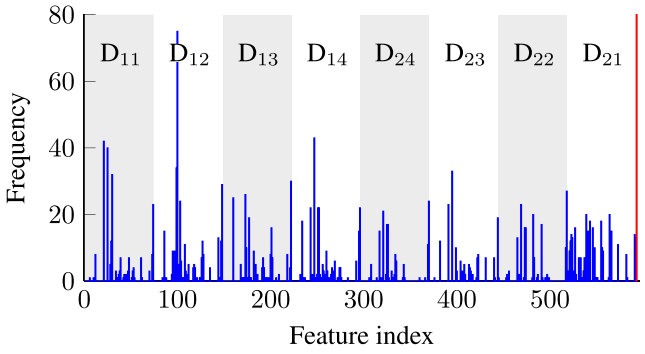


**FIGURE 10. Transducer-dependent feature frequency at 100-fold SFS with 1NN classifier and BAC* as OC.**

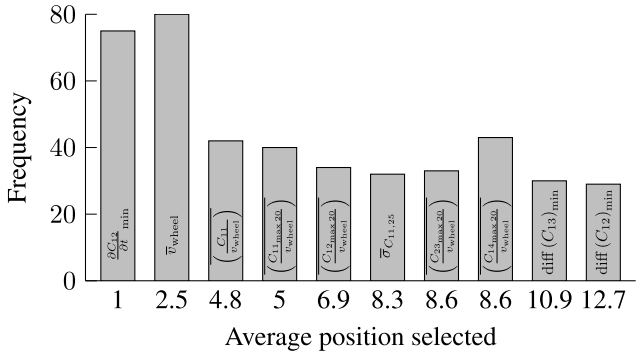


**FIGURE 11. Frequency over average position of most frequent selected features at 100-fold SFS with 1NN classifier and BAC* as OC.**

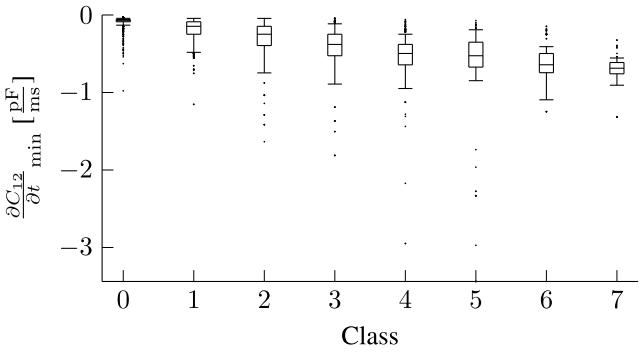


**FIGURE 12. Box-and-whisker plot of the feature $\frac{\partial C_{12}}{\partial t}_{\min}$. The whiskers representing values 1.5 times the interquartile range above the upper respectively below the lower quartile. Any other value is assumed to be an outlier, marked as a dot.**

Since SFS is not deterministic for varying data sets due to cross-validation, we perform a total of 100 SFSs with the chosen classifier and examine the frequency, relevance, and required amount of features.

Except mean wheel speed, our feature space comprises two dimensions, 8 transducers and 74 features, resulting in a total of 593 features. The features are generated by statistical attributes and data vectors related to the measured capacitance, wheel speed, and time. Table 7 gives an overview of the feature set applied to each transducer. It provides a connection between the statistical attributes and the evaluated vectors. Besides common statistical features like minimum, maximum, or mean, implemented for the whole time window, more specific features comprising a fixed number of sample points $s$ are implemented, with a particular focus on the capacitance's standard deviation SD. Another notable feature is represented by diff, which describes the largest or smallest change between two consecutive sample points within a time window.

In Fig. 10 the transducer-dependent feature frequency over the feature index of 100-fold SFS is shown. In addition, the red bar with index 593 represents the feature mean wheel speed. During the 100 iterations, on average 18.49 features per SFS and a maximum of 30 features are selected. Furthermore, in total 226 of the 593 features are selected with 63 of them being selected more than ten times, demonstrating the non-deterministic behavior of SFS. Moreover, a distribution over both dimensions of the selected features can be seen from the figure. Although this figure does not yet allow conclusions to be drawn about the importance of each transducer, it does provide an indicator of the array's relevance with regard to classifier performance. In addition, the mean wheel speed's selection frequency is noticeable. Even though this feature on its own cannot classify the data, since the decision-criterion for road wetness is the transducer's capacitance, it is selected in four fifths of the iterations. As outlined in Section V, wheel speed is correlated with the amount and size of thrown up water droplets impinging on the transducer, which explains its importance for road surface wetness classification.

Fig. 11 summarizes the ten most frequently selected features during 100-fold SFS. It shows the frequency over the average position selected in SFS for each feature. The most frequent feature, mean wheel speed, is selected 80 times on average at position 2.5. Furthermore, there are five other speed-related features in the top ten, each selected in more than a third of the SFSs. Four of these features represent the highest 20% values' mean of the capacitance and wheel speed's quotient and the other one the quotient's mean for the whole time window. These features are selected

comparatively early in SFS, again underlining the wheel speed's importance with regard to the classifier performance.

There is only one feature selected earlier on average, which represents the time window's minimum capacitance increase between two samples in relation to the time of transducer $D_{12}$. If this feature is selected, it is in the first position, which occurs in three quarters of the iterations. Consequently, this feature is apparently best suited to classify on its own with a BAC* of approximately 0.86 on average. Fig. 12 shows the data distribution in a box-and-whisker plot of the feature for the eight classes. Class dry is unique in position and has a comparably small interquartile range indicating a low data variance and therefore the higher classifier performance depicted in Fig. 9. As the class index increases, the feature's median decreases. In addition, each classes data distribution is individual and in a narrow value range providing a reliable class prediction.

If the feature from Fig. 12 is not selected first, similar features regarding the capacitance increase are selected instead, which refer to $D_{12}$ or $D_{13}$ in 99%. The lowest-performing feature (BAC* around 0.81) selected at first position refers to $D_{14}$ and represents the time window's maximum capacitance increase. Thus, all features selected at first position refer to transducers of Design 1 (see Table 1), which seem to be more suitable to classify on their own (more on this in Section VI-D).

Two additional features, shown in Fig. 11, also relate to the capacitance increase. As figured out in Section V, the capacitance curve's gradient is correlated with water film thickness. Therefore, these features provide an increase in classifier performance resulting in a high selection frequency. The remaining feature of the ten most frequently selected represents the capacitance curve's mean standard deviation for intervals of 25 sample points. This kind of feature is particularly relevant if the road surface is dry or once the speed-/wetness-related maximum is reached. In those situations, they significantly complement the features described above.

A similar picture emerges for the transducer-independent consideration of the most selected features. Here, four capacitance increase-, three standard deviation- and three speed-related features are among the top ten, illustrating their importance and complementarity. On the contrary, features representing capacitance by statistics like minimum, maximum, or mean are selected more rarely, since their information gain alone is too insignificant and disadvantageous compared to the features above.

A more detailed analysis of the two highest-performing classifiers of 100-fold SFS confirms the assumptions previously made. For both SFSs, a balanced ratio between the three most frequent feature types described above is given including seven of the ten most frequently selected features from Fig. 11. Furthermore, both selections contain merely one feature representing capacitance by statistics like minimum or maximum. While the second-best classifier includes 17 features at a BAC* of 0.92, the best contains 28 features

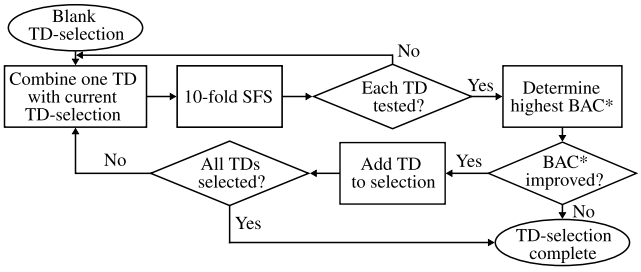


**FIGURE 13.** Flow chart for the approach of forward transducer selection.

**TABLE 8.** Performance (BAC*) history of forward transducer selection excluding the feature mean wheel speed.

| $i$ | $D_{11}$ | $D_{12}$ | $D_{13}$ | $D_{14}$ | $D_{24}$ | $D_{23}$ | $D_{22}$ | $D_{21}$ |
|---|---|---|---|---|---|---|---|---|
| 1 | 0.8267 | **0.8608** | 0.8531 | 0.8325 | 0.8009 | 0.8107 | 0.8135 | 0.8213 |
| 2 | **0.8915** | - | 0.8618 | 0.8611 | 0.8602 | 0.8672 | 0.8613 | 0.8802 |
| 3 | - | - | 0.8612 | 0.8693 | 0.8976 | 0.8985 | 0.8959 | **0.9098** |
| 4 | - | - | 0.9072 | 0.9092 | 0.9093 | **0.9116** | 0.9097 | - |
| 5 | - | - | 0.9116 | **0.9130** | 0.9113 | - | 0.9102 | - |
| 6 | - | - | 0.9127 | - | **0.9138** | - | 0.9119 | - |

at a BAC* of 0.95. Thus, the latter can even outperform the classifier presented above and with a BAC of 0.93 reach the same performance as binary classifiers from related research (see Section VI-B). In addition, a consideration of the transducer-dependent features gives further evidence for the electrode array's importance. After eight selected features, the best classifier already includes features from six different transducers. At position 22 and 23, features from the remaining transducers ($D_{14}$ and $D_{24}$) are selected. However, these features only result in a marginal improvement. A similar picture emerges with the second-best classifier. Here, features from six different transducers excluding $D_{22}$ and $D_{24}$ are selected. In the following section, a more detailed consideration follows with regard to each transducer's relevance.

### D. FORWARD TRANSDUCER SELECTION

As shown in the previous section, features from both dimensions, including the eight transducers, are selected during SFS. In order to study each transducer's contribution to classifier performance, we take a closer look at them within this section. For the study, we again apply 1NN with BAC* as OC and separate the feature space into eight parts, respectively nine parts considering mean wheel speed. Furthermore, we introduce forward transducer selection (FTS), which is based on the wrapper method known from feature selection and successively generates combinations of the available transducers.

Fig. 13 shows the flow chart for FTS. Each remaining (initially eight) transducer's features space is combined individually with the previously selected transducers' feature space (initially blank) and ten SFSs are performed respectively. Subsequently, BAC* is determined by ten-fold cross-validation for every SFS. Once all transducers

have been tested, the highest performing classifier is determined and compared to the previous transducer selection's classifier performance. If BAC* can be improved, the causing transducer is added to the selection. This is continued until all transducers have been added or BAC* cannot be improved further by adding a transducer.

In Table 8, the performance history of FTS excluding mean wheel speed is summarized. The first sensor to be selected with a BAC* of 0.86 is $D_{12}$, which therefore also represents the most suitable single sensor solution with considerable performance. In comparison, only $D_{13}$ which is of the same electrode design and positioned adjacent above $D_{12}$ can nearly reach that performance. Due to their redundancy, other transducers are preferred in further FTS and $D_{13}$ is not selected despite the high performance as a single sensor.

Furthermore, the table reveals design-related advantages with regard to a single sensor setup. All transducers of Design 1 (see Table 1) show higher performance than those of Design 2. This may be attributed to the design properties since Design 1 provides a higher penetration depth providing the measurements of water spray in a wider range (see Section III-B). Thus, Design 2 offers more complementary qualities in the proposed transducer array. In addition, the results also indicate position-related advantages for a single sensor setup. As the transducer height increases at the front wheel arch liner's rear-facing side ($D_{12}$ to $D_{14}$, see Fig. 3), the classifier performance decreases. Since droplet size and amount decrease as the spray-off angle increases, $D_{12}$ shows advantages regarding the classification across the entire wetness levels. Furthermore, the position at the transition to the vehicle's underbody ($D_{11}$) shows drawbacks as a single sensor. The above can be confirmed by the results from Section VI-C, where 83% of the first selected features in 100-fold SFS referred to $D_{12}$ and the remainder to $D_{13}$ or $D_{14}$.

On the contrary, $D_{11}$ shows the best complementary characteristics and is selected second with a performance increase of around 0.03. Since the position is less attracted to impinging water droplets in comparison (see Section V), its redundancy to transducers at the front wheel arch liner's rear-facing side is comparatively low. The same holds for $D_{21}$, which yields the second-highest performance increase and is selected third for the same reason. Subsequently, $D_{23}$, $D_{14}$ and $D_{24}$ are selected. Although the performance increase is lower than before, they can significantly improve the classifier. In total, six transducers, three of each design, are selected covering all vertical positions.

As shown in Section VI-C, mean wheel speed is a feature with high selection frequency, even though it cannot classify wetness on its own and other speed-related features are available. In order to study its influence on required transducers and classifier performance, we repeat FTS including the feature mean wheel speed. Table 9 summarizes the corresponding performance history. In comparison to Table 8, there is a significant increase in classifier performance for the transducers at the front wheel arch liner's rear-facing side with regard to a single sensor setup. Since Design 2 shows its advantages for low amounts of water droplets (see Section VI-D), and droplet size and amount decrease as the spray-off angle increases, especially $D_{23}$ and $D_{24}$ can benefit from the additional information. Nevertheless, the most suitable transducer selected first is still $D_{12}$ with a BAC* of 0.87.

**TABLE 9. Performance (BAC*) history of forward transducer selection including the feature mean wheel speed.**

| $i$ | $D_{11}$ | $D_{12}$ | $D_{13}$ | $D_{14}$ | $D_{24}$ | $D_{23}$ | $D_{22}$ | $D_{21}$ |
|---|---|---|---|---|---|---|---|---|
| 1 | 0.8263 | **0.8662** | 0.8543 | 0.8337 | 0.8402 | 0.8319 | 0.8140 | 0.8211 |
| 2 | **0.9060** | - | 0.8682 | 0.8859 | 0.8847 | 0.8717 | 0.8874 | 0.9027 |
| 3 | - | - | 0.9029 | 0.9032 | 0.9008 | 0.9041 | 0.9015 | **0.9124** |
| 4 | - | - | 0.9138 | 0.9137 | 0.9161 | 0.9149 | **0.9170** | - |
| 5 | - | - | 0.9155 | 0.9166 | 0.9180 | **0.9220** | - | - |

Similar to the previous FTS, $D_{11}$ and $D_{21}$ are selected subsequently. This is followed by the selection of $D_{22}$ and $D_{23}$, which yield a higher performance increase compared to the features selected on similar positions in the previous FTS. In total, one transducer less is selected and a performance increase of nearly 0.01 can be yielded by adding the additional feature. Furthermore, no upper transducer is selected, which might be attributed to the additional information provided by the mean wheel speed. Thus, the vertical arrangement does not seem to be as decisive as before for the studied wheel speeds.

In brief, to a certain extent, the array's individual transducers can contribute significantly to classifier performance, just as appropriate statistical features do. With regard to the required accuracy and available implementation space, a trade-off exists between classifier performance and transducer number. According to the findings, a single-sensor solution is also conceivable as a considerable BAC* performance of 0.87 is achievable.

## VII. CONCLUSION

In this paper, a novel concept for road surface wetness quantification has been proposed. The concept is based on a $2 \times 4$-planar capacitive transducer array designed for the front wheel arch liner's rear-facing side enabling to detect water ejected by the tires. In an experimental study on an asphalt circuit, the spray's correlation with wheel speed and road surface wetness has been confirmed for the studied wheel speeds. Furthermore, the reliable assessment of wetness-related dependencies with the proposed capacitive sensor system has been shown. The results have also revealed significant differences between the transducer designs and positions as the amount and size of water droplets vary along the tire's rotation confirming the array's relevance with regard to wetness quantification.

In addition, different learning algorithms and optimization criteria for automatically classifying road surface wetness into eight classes have been studied with the experimental data. An extended version of the balanced accuracy as optimization criterion and 1NN classifier has achieved the highest performance. The overall best classifier yields a BAC

of 0.93 and can thereby reach the same performance as binary classifiers from related research. Furthermore, a binary version of our classifier yields a BAC of 0.998 confirming the potential of our concept to almost perfectly distinguish between dry and wet road surfaces for the studied wheel speeds. One key aspect of classifier performance can be attributed to the features selected. A balanced ratio between capacitance increase-, standard deviation- and speed-related feature types provides the highest classifier performance. In addition, the feature average wheel speed can significantly improve classifier performance. Furthermore, up to a certain extent, the array's individual transducers can significantly improve classifier performance with design- and position-related advantages.

Future work involves the investigation of higher wheel speeds and feature selection algorithms with regard to classifier performance.

## REFERENCES


[1] S. Bundesamt, "Verkehrsunfälle—Fachserie 8 Reihe 7—2018," Federal Stat. Office (Destatis), Wiesbaden, Germany, Tech. Rep. 2080700197004, Jul. 2019.

[2] C. Ahn, H. Peng, and H. E. Tseng, "Robust estimation of road frictional coefficient," *IEEE Trans. Control Syst. Technol.*, vol. 21, no. 1, pp. 1–13, Jan. 2013.

[3] C.-G. Wallman and H. Åström, *Friction Measurement Methods and the Correlation Between Road Friction and Traffic Safety A Literature Review*. Linköping, Sweden: Swedish National Road and Transport Research Institute, 2001.

[4] H. Brodsky and A. S. Hakkert, "Risk of a road accident in rainy weather," *Accident Anal. Prevention*, vol. 20, no. 3, pp. 161–176, Jun. 1988.

[5] R. Lamm, E. M. Choueiri, and T. Mailaender, "Comparison of operating speeds on dry and wet pavements of two-lane rural highways," *Transp. Res. Rec.*, vol. 1280, no. 8, pp. 199–207, 1990.

[6] A. G. Kokkalis and O. K. Panagouli, "Fractal evaluation of pavement skid resistance variations. I: Surface wetting," *Chaos, Solitons Fractals*, vol. 9, no. 11, pp. 1875–1890, Nov. 1998.

[7] W. R. Stohner, "Speeds of passenger cars on wet and dry pavements," *Highway Res. Board Bull.*, vol. 139, pp. 79–84, Oct. 1956.

[8] D. J. Fagnant and K. Kockelman, "Preparing a nation for autonomous vehicles: Opportunities, barriers and policy recommendations," *Transp. Res. A, Policy Pract.*, vol. 77, pp. 167–181, Jul. 2015.

[9] M. Aldibaja, N. Suganuma, and K. Yoneda, "Robust intensity-based localization method for autonomous driving on Snow–Wet road surface," *IEEE Trans. Ind. Informat.*, vol. 13, no. 5, pp. 2369–2378, Oct. 2017.

[10] E. Arnold, O. Y. Al-Jarrah, M. Dianati, S. Fallah, D. Oxtoby, and A. Mouzakitis, "A survey on 3D object detection methods for autonomous driving applications," *IEEE Trans. Intell. Transp. Syst.*, vol. 20, no. 10, pp. 3782–3795, Oct. 2019.

[11] S. Zang, M. Ding, D. Smith, P. Tyler, T. Rakotoarivelo, and M. A. Kaafar, "The impact of adverse weather conditions on autonomous vehicles: How rain, snow, fog, and hail affect the performance of a self-driving car," *IEEE Veh. Technol. Mag.*, vol. 14, no. 2, pp. 103–111, Jun. 2019.

[12] G. Cheng, Z. Wang, and J. Y. Zheng, "Modeling weather and illuminations in driving views based on big-video mining," *IEEE Trans. Intell. Veh.*, vol. 3, no. 4, pp. 522–533, Dec. 2018.

[13] M. Bijelic, T. Gruber, and W. Ritter, "Benchmarking image sensors under adverse weather conditions for autonomous driving," in *Proc. IEEE Intell. Vehicles Symp. (IV)*, Jun. 2018, pp. 1773–1779.

[14] G. Pan, L. Fu, R. Yu, and M. Muresan, "Evaluation of alternative pre-trained convolutional neural networks for winter road surface condition monitoring," in *Proc. 5th Int. Conf. Transp. Inf. Saf. (ICTIS)*, Jul. 2019, pp. 614–620.

[15] P. Jonsson, "Classification of road conditions: From camera images and weather data," in *Proc. IEEE Int. Conf. Comput. Intell. Meas. Syst. Appl. (CIMSA) Process.*, Sep. 2011, pp. 1–6.

[16] A. Kuehnle and W. Burghout, "Winter road condition recognition using video image classification," *Transp. Res. Rec., J. Transp. Res. Board*, vol. 1627, no. 1, pp. 29–33, Jan. 1998.

[17] W. Hetzner, "Recognition of road conditions with active and passive millimeter-wave sensors," *Frequenz*, vol. 38, nos. 7–8, pp. 179–185, 1984.

[18] V. V. Viikari, T. Varpula, and M. Kantanen, "Road-condition recognition using 24-GHz automotive radar," *IEEE Trans. Intell. Transp. Syst.*, vol. 10, no. 4, pp. 639–648, Dec. 2009.

[19] F. Holzwarth and U. Eichhorn, "Non-contact sensors for road conditions," *Sens. Actuators A, Phys.*, vols. 37–38, pp. 121–127, Jun. 1993.

[20] J. Casselgren, "Road surface classification using near infrared spectroscopy," Ph.D. dissertation, Dept. Eng. Sci. Math., Luleå Tekniska Univ., Luleå, Sweden, 2007.

[21] G. Lufft, *Operating Manual MARWIS-UMB/STARWIS-UMB*. Enkenbach-Alsenborn, Germany: Messund Regeltechnik GmbH, 2019.

[22] I. Abdic, L. Fridman, D. E. Brown, W. Angell, B. Reimer, E. Marchi, and B. Schuller, "Detecting road surface wetness from audio: A deep learning approach," in *Proc. 23rd Int. Conf. Pattern Recognit. (ICPR)*, Dec. 2016, pp. 3458–3463.

[23] J. Alonso, J. López, I. Pavón, M. Recuero, C. Asensio, G. Arcas, and A. Bravo, "On-board wet road surface identification using tyre/road noise and support vector machines," *Appl. Acoust.*, vol. 76, pp. 407–415, Feb. 2014.

[24] M. Kalliris, S. Kanarachos, R. Kotsakis, O. Haas, and M. Blundell, "Machine learning algorithms for wet road surface detection using acoustic measurements," in *Proc. IEEE Int. Conf. Mechatronics (ICM)*, Mar. 2019, pp. 265–270.

[25] H.-J. Görich, S. Jacobi, and U. Reuter, "Ermittlung des aktuellen Kraftschluß potentials eines Pkws im Fahrbetrieb," in *Proc. VDI BERICHTE*, vol. 1088, 1993, pp. 299–328.

[26] S. Jacobi, "Sensor zum Erfassen der Benetzung einer Fahrbahn," German Patent DE19 543 137 A1, May 18, 1993.

[27] B. Schmiedel, F. Gauterin, and H.-J. Unrau, "Study of system layouts for road wetness quantification via tire spray," *Automot. Engine Technol.*, vol. 4, nos. 1–2, pp. 63–73, Jun. 2019.

[28] Dr Ing Porsche AG. (Jan. 2019). *High Driving Stability Even in the Rain*. [Online]. Available: https://newsroom.porsche.com/en/products/porsche-911-new-eigth-generation-992-timeless-machine-design-icon-wet-mode-detecting-wet-road-conditions-16857.html

[29] HELLA GmbH & Co. KGaA. (Nov. 2019). *Shake Technology From HELLA Goes Into Series Production*. [Online]. Available: https://www.hella-pagid.com/press/en/Technology-Products-26-11-2019-18509.html

[30] A. Troiano, E. Pasero, and L. Mesin, "New system for detecting road ice formation," *IEEE Trans. Instrum. Meas.*, vol. 60, no. 3, pp. 1091–1101, Mar. 2011.

[31] C. Baby K. and B. George, "A capacitive ice layer detection system suitable for autonomous inspection of runways using an ROV," in *Proc. IEEE Int. Symp. Robotic Sensors Environ. Process.*, Nov. 2012, pp. 127–132.

[32] J. Döring, L. Tharmakularajah, J. Happel, and K.-L. Krieger, "A novel approach for road surface wetness detection with planar capacitive sensors," *J. Sensors Sensor Syst.*, vol. 8, no. 1, pp. 57–66, Jan. 2019.

[33] X. Hu and W. Yang, "Planar capacitive sensors–designs and applications," *Sensor Rev.*, vol. 30, no. 1, pp. 24–39, Jan. 2010.

[34] A. V. Mamishev, K. Sundara-Rajan, F. Yang, Y. Du, and M. Zahn, "Interdigital sensors and transducers," *Proc. IEEE*, vol. 92, no. 5, pp. 808–845, May 2004.

[35] J. Mizuguchi, J. C. Piai, J. A. de França, M. B. de Morais França, K. Yamashita, and L. C. Mathias, "Fringing field capacitive sensor for measuring soil water content: Design, manufacture, and testing," *IEEE Trans. Instrum. Meas.*, vol. 64, no. 1, pp. 212–220, Jan. 2015.

[36] R. N. Dean, A. K. Rane, M. E. Baginski, J. Richard, Z. Hartzog, and D. J. Elton, "A capacitive fringing field sensor design for moisture measurement based on printed circuit board technology," *IEEE Trans. Instrum. Meas.*, vol. 61, no. 4, pp. 1105–1112, Apr. 2012.

[37] X. B. Li, S. D. Larson, A. S. Zyuzin, and A. V. Mamishev, "Design of multichannel fringing electric field sensors for imaging. Part I. General design principles," in *Proc. Conf. Rec. IEEE Int. Symp. Electr. Insul.*, Sep. 2004, pp. 406–409.

[38] H.-C. Wang, A. Zyuzin, and A. V. Mamishev, "Measurement of coating thickness and loading using concentric fringing electric field sensors," *IEEE Sensors J.*, vol. 14, no. 1, pp. 68–78, Jan. 2014.

[39] A. Savkoor, "Tribology of tyre traction on dry and wet roads," in *Proc. 17th Leeds–Lyon Symp. Tribol.-Veh. Tribol.*, 1991, pp. 213–228.

[40] V. E. Gough, "Friction of rubber on lubricated surfaces," in *Contribution to Discussion of Paper*, vol. 36, D. Tabor, Ed. Paris, France: Revue Générale du Caoutchouc, 1959, p. 1409.

[41] D. F. Moore, "A review of squeeze films," *Wear*, vol. 8, no. 4, pp. 245–263, Jul. 1965.
[42] W. E. Meyer, *Frictional Interaction Tire Pavement*, vol. 793. West Conshohocken, PA, USA: ASTM International, 1983.
[43] R. H. Smith, *Analyzing Friction Design Rubber Products Their Paired Surface*. Boca Raton, FL, USA: CRC Press, 2008.
[44] D. H. Weir, J. F. Strange, and R. K. Heffley, "Reduction of adverse aerodynamic effects of large trucks, Volume I. Technical report," Federal Highway Admin., Washington, DC, USA, Tech. Rep. FHWA-RD-79-84, 1978.
[45] R. M. Clarke, *Heavy Truck Splash and Spray Suppression: Near and Long Term Solutions*. Warrendale, PA, USA: SAE Transactions, 1983, pp. 665–675.
[46] T. Schütz, *Hucho-Aerodynamik des Automobils: Strömungsmechanik, Wärmetechnik, Fahrdynamik, Komfort*. Wiesbaden, Germany: Springer-Verlag, 2013.
[47] I. Spruß, "Ein beitrag zur untersuchung der kraftfahrzeugverschmutzung in experiment und simulation," Ph.D. dissertation, Dept. Verbrennungsmotoren und Kraftfahrwesen, Univ. Stuttgart, Stuttgart, Germany, 2016.
[48] A. Kabanovs, A. Garmory, M. Passmore, and A. Gaylard, "Investigation into the dynamics of wheel spray released from a rotating tyre of a simplified vehicle model," *J. Wind Eng. Ind. Aerodyn.*, vol. 184, pp. 228–246, Jan. 2019.
[49] V. Strohbücker, R. Niesner, and F. Joos, "Simulation method for vehicle tire water spraying behavior," in *Proc. Int. Stuttgarter Symp.* Wiesbaden, Germany: Springer, 2018, pp. 1393–1409.
[50] *FDC2x1x EMI-Resistant 28-Bit,12-Bit Capacitance-to-Digital Converter for Proximity and Level Sensing Applications*, Texas Instruments, Dallas, TX, USA, 2015.
[51] Y. Sun, A. K. Wong, and M. S. Kamel, "Classification of imbalanced data: A review," *Int. J. Pattern Recognit. Artif. Intell.*, vol. 23, no. 4, pp. 687–719, 2009.
[52] S. Kotsiantis, D. Kanellopoulos, and P. Pintelas, "Handling imbalanced datasets: A review," *GESTS Int. Trans. Comput. Sci. Eng.*, vol. 30, no. 1, pp. 25–36, 2006.
[53] S. Boughorbel, F. Jarray, and M. El-Anbari, "Optimal classifier for imbalanced data using Matthews correlation coefficient metric," *PLoS ONE*, vol. 12, no. 6, Jun. 2017, Art. no. e0177678.
[54] G. M. Weiss, "Mining with rarity: A unifying framework," *ACM SIGKDD Explor. Newslett.*, vol. 6, no. 1, pp. 7–19, Jun. 2004.
[55] H. Carrillo, K. H. Brodersen, and J. A. Castellanos, "Probabilistic performance evaluation for multiclass classification using the posterior balanced accuracy," in *Proc. 1st Iberian Robot. Conf.* Cham, Switzerland: Springer, 2014, pp. 347–361.
[56] L. Mosley, "A balanced approach to the multi-class imbalance problem," Ph.D. dissertation, Dept. Ind. Manuf. Syst. Eng., Iowa State Univ., Ames, IA, USA, 2013.
[57] J. D. Kelleher, B. M. Namee, and A. D'arcy, *Fundamentals of Machine Learning for Predictive Data Analytics: Algorithms, Worked Examples, and Case Studies*. Cambridge, MA, USA: MIT Press, 2015.
[58] B. W. Matthews, "Comparison of the predicted and observed secondary structure of T4 phage lysozyme," *Biochim. Biophys. Acta-Protein Struct.*, vol. 405, no. 2, pp. 442–451, Oct. 1975.
[59] J. Gorodkin, "Comparing two K-category assignments by a K-category correlation coefficient," *Comput. Biol. Chem.*, vol. 28, nos. 5–6, pp. 367–374, Dec. 2004.
[60] G. Jurman, S. Riccadonna, and C. Furlanello, "A comparison of MCC and CEN error measures in multi-class prediction," *PLoS ONE*, vol. 7, no. 8, Aug. 2012, Art. no. e41882.
[61] P. Jonsson, J. Casselgren, and B. Thornberg, "Road surface status classification using spectral analysis of NIR camera images," *IEEE Sensors J.*, vol. 15, no. 3, pp. 1641–1656, 2015.
[62] V. Kotu and B. Deshpande, *Predictive Analytics Data Mining: Concepts Practice With Rapidminer*. Burlington, MA, USA: Morgan Kaufmann, 2014.
[63] Z. Yu, F. Haghighat, B. C. M. Fung, and H. Yoshino, "A decision tree method for building energy demand modeling," *Energy Buildings*, vol. 42, no. 10, pp. 1637–1646, Oct. 2010.
[64] G. James, D. Witten, T. Hastie, and R. Tibshirani, *An Introduction to Statistical Learning*, vol. 112. New York, NY, USA: Springer, 2013.
[65] K. Chomboon, P. Chujai, P. Teerarassammee, K. Kerdprasop, and N. Kerdprasop, "An empirical study of distance metrics for k-nearest neighbor algorithm," in *Proc. 2nd Int. Conf. Ind. Appl. Eng.*, 2015, pp. 280–285.
[66] I. H. Witten, C. J. Pal, E. Frank, and M. A. Hall, *Data Mining: Practical Machine Learning Tools Techniques*, 4th ed. Cambridge, MA, USA: Morgan Kaufmann, 2017.
[67] I. Guyon and A. Elisseeff, "An introduction to variable and feature selection," *J. Mach. Learn. Res.*, vol. 3, pp. 1157–1182, Jan. 2003.
[68] A. Marcano-Cedeno, J. Quintanilla-Domínguez, M. Cortina-Januchs, and D. Andina, "Feature selection using sequential forward selection and classification applying artificial metaplasticity neural network," in *Proc. 36th Annu. Conf. Ind. Electron. Soc.*, Oct. 2010, pp. 2845–2850.

**JAKOB DÖRING** received the B.Sc. and M.Sc. degrees in electrical and information engineering from the University of Bremen, Germany, in 2014 and 2017, respectively, where he is currently pursuing the Ph.D. degree with the Institute of Electrodynamics and Microelectronics. His research interests include capacitive sensors and the classification of road surface wetness.

**ANDREAS BEERING** received the B.Sc. and M.Sc. degrees in electrical and information engineering from the University of Bremen, Germany, in 2015 and 2017, respectively, where he is currently pursuing the Ph.D. degree with the Institute of Electrodynamics and Microelectronics. His research interests include signal processing and classification of vibration signals.

**JULIA SCHOLTYSSEK** received the B.Sc. and M.Sc. degrees in electrical engineering and management from the University of Bremen, Germany, in 2019 and 2021, respectively, where she is currently pursuing the Ph.D. degree with the Institute of Electrodynamics and Microelectronics. Her research interests include classification and forecasting based on vibration signals.

**KARL-LUDWIG KRIEGER** received the Ph.D. degree in electrical engineering from the University of Bremen, Germany, in 1999. From 1998 to 2009, he worked as a Manager in the field of function and algorithm development for powertrain systems at Daimler AG, Stuttgart. Since 2009, he has been a Full Professor with the Chair of Electronic Vehicle and Mobility Systems, University of Bremen.